Vibrational and electronic spectra of EuF_6^{3-}

1997 J. Phys.: Condens. Matter 9 7817

(http://iopscience.iop.org/0953-8984/9/37/013)

J. Phys.: Condens. Matter **9** (1997) 7817–7836. Printed in the UK PII: S0953-8984(97)79407-4

Vibrational and electronic spectra of EuF_6^{3-}

Peter A Tanner†, Liu Yulong†, Norman M Edelstein‡, Keith M Murdoch‡ and Nicholas M Khaidukov§

† Department of Biology and Chemistry, City University of Hong Kong, Tat Chee Avenue, Kowloon, Hong Kong‖

‡ Chemical Sciences Division, Lawrence Berkeley National Laboratory, 1 Cyclotron Road, Berkeley, CA 94720, USA¶

§ Russian Academy of Sciences, N S Kurnakov Institute of General and Inorganic Chemistry, 31 Leninskii Prospekt, 117907 Moscow, Russia

Received 8 November 1996, in final form 21 April 1997

Abstract. Single crystals of Cs_2NaYF_6 doped with molar concentrations of Eu^{3+} between 0.1 and 20% have been synthesized by the hydrothermal method, and studied by absorption, excitation and luminescence spectroscopy at temperatures down to 4 K. The observed spectral features were consistently assigned with reference to those of the corresponding europium hexachloroelpasolite. No distortion from octahedral symmetry was evident for the Eu^{3+} site in the 0.1 mol%-doped Cs_2NaYF_6 crystal, but small splittings of magnetic dipole zero-phonon lines in the spectra of the 20%-doped crystals are observed below 20 K. The vibrational behaviour of EuF_6^{3-} has been interpreted, and the energy-level scheme of the Eu^{3+} ion was deduced from the observed and inferred zero-phonon-line positions in the optical spectra. A parametrized Hamiltonian was fitted to 21 crystal-field levels of Eu^{3+} in Cs_2NaYF_6. The fourth- and sixth-degree crystal-field parameters were about 1.6 times larger than for $Cs_2NaEuCl_6$. The temperature shifts of the crystal-field levels were found to be negative, in contrast to the mostly positive shifts previously reported for actinide systems in octahedral symmetry, and were largely determined by the changes in the Slater parameters rather than the crystal-field parameters. A preliminary study has been made of the decay kinetics of the ^5D_J ($J = 0, 1, 2$) levels. $^5D_2$ is quenched by a cross-relaxation mechanism, and $^5D_1$ also by a thermally activated mechanism. The lifetime of $^5D_0$ does not exhibit a noticeable temperature or concentration dependence.

1. Introduction

The energy levels [1] and energy-transfer processes [2–5] in lanthanide hexachloroelpasolites [6], $Cs_2NaLnCl_6$ (Ln = lanthanide element), have been extensively investigated, but the range of optical emission and absorption studies of the corresponding hexafluoro-compounds is more limited. This has been largely due to technical problems in the synthesis. Two main preparative techniques have previously been employed to synthesize A_2BMF_6 compounds: the high-temperature reaction of a mixture of the appropriate anhydrous fluorides (or hydrogen fluorides), sometimes compressed into a pellet, in an inert container; or the direct fluorination of the corresponding chloro-compound [7–12]. The structure of the product, *elpasolite* (K_2NaAlF_6, $Fm3m$-type), *cryolite* (Na_3AlF_6, $P2_1/m$-type), or some other type, has been shown to depend upon the value of the tolerance factor [11] and upon the electronic

‖ E-mail: bhtan@cityu.edu.hk.

¶ E-mail: nedel@actinide.lbl.gov.

0953-8984/97/377817+20$19.50

structure of the M^{3+} ion [13]. Phase transitions occur for crystals of several lanthanide-ion hexafluoroelpasolites on cooling from room temperature, and the nature of these has been studied by different techniques [13–18]. Their magnetic properties [19–21] and solid-state nmr spectra [22, 23] have also received attention. Studies of luminescence [24–26] and absorption spectra [12, 27] of hexafluoroelpasolites have been fragmentary. Recently, however, a parametrization of extensive energy-level data-sets for terbium elpasolites, obtained from one- and two-photon spectroscopy, has been reported [28].

Temperature shifts of the energies of electronic levels, relative to the electronic ground state, are usually of minor importance for lanthanide hexachloroelpasolites, so, unlike the intensity changes of spectral transitions with temperature, they have not been considered previously. The stronger crystal-field (CF) interaction for actinide ions leads to much larger changes in the energies of CF levels with temperature. Satten and co-workers [29] assumed that the shifts in the optical spectra of Cs_2UX_6 (X = Br, Cl) were mainly due to the increase in CF accompanying the contraction of the lattice on cooling the crystal, and examined the derivatives of the energies (relative to the ground level) with respect to the parameters B_0^4 and B_0^6. Two Γ_1–Γ_1 transitions were found to exhibit *negative* shifts with temperature (i.e. $E(295\ \mathrm{K}) > E(4.2\ \mathrm{K})$) and this confirmed the assignment of the terminal Γ_1 levels. In addition, the sign and magnitudes of the energy-level shifts from Cs_2UBr_6 to Cs_2UCl_6 were found to be related to the temperature shifts of one of these compounds. The energy-level shifts from Cs_2NaYCl_6:Eu^{3+} to Cs_2NaYF_6:Eu^{3+} (the 3+ charge is omitted hereafter), and the temperature shifts in the Cs_2NaYF_6 host are discussed in section 3.5.

The luminescence from the $^5D_0$ state of $Cs_2NaEuCl_6$ has been investigated [4] and the non-exponential decay was attributed to quenching of Eu^{3+} ions situated at defect sites adjacent to interstitial water molecules. The appearance of the weak $^7F_0 \rightarrow {}^5D_0$ absorption transition [30] is significantly different from the reported excitation spectrum [4], which may indicate the role of more than one species in the latter. Luminescence from $^5D_1$ in $Cs_2NaEuCl_6$ was found to follow exponential decay and to exhibit concentration quenching. The calculated energy migration rate in dilute Cs_2NaYCl_6:Eu via a magnetic dipole–magnetic dipole (MD–MD) interaction [31] is in agreement with experiment [4]. The cross-relaxation mechanism for Eu^{3+} transiting from $^5D_1$ to $^5D_0$ was attributed to a thermally activated process in which one Eu^{3+} is initially in the $^7F_1$ state or an excited vibrational level of the ground state [4]. It is noted herein that the non-thermally activated (EQ–MD–EQ, where EQ = electric quadrupole) three-body process in which two Eu^{3+} are excited to $(^7F_2)\Gamma_3$ from the $^7F_0$ ground state, whilst the third Eu^{3+} relaxes from $^5D_1$ to $^5D_0$, is resonant. Although the temperature shifts of energy levels would lead to changes in the energy-transfer rate from $^5D_1$ under this mechanism, it is unlikely that they would account for the *observed* changes in transfer rate. Non-radiative multi-phonon decay from $^5D_1$ to $^5D_0$ cannot occur via a *single* quantum of a τ_{1g}-symmetry-promoting mode and multiple quanta of an α_{1g} accepting mode (section 3.2, equation (4)).

The main aim of the present study was to synthesize and investigate the vibrational behaviour and one-photon electronic spectra of the europium (III) hexafluoroelpasolite system, in which the lanthanide ion has the f^6 electron configuration. The comparison of the energy levels with those of the corresponding hexachloroelpasolite, Cs_2NaYCl_6:Eu, was also of interest. These aims have been accomplished using the Eu^{3+} ion doped into cubic Cs_2NaYF_6 at several different concentrations. In addition, we have made a preliminary study of the luminescence decay kinetics of this system.

2. Experimental procedure

$Cs_2NaY_{1-x}Eu_xF_6$ (with the nominal concentrations $x = 0.001$, 0.004, 0.04 and 0.2) was synthesized by the reaction of aqueous solutions of CsF and NaF with mixtures of Eu_2O_3 and Y_2O_3 (99.995%) at a temperature of 750 K and pressures of 100–150 MPa [32]. The phase homogeneity of the crystals obtained and the perfection of the crystal lattice were tested by x-ray powder diffraction. The doped single crystals were synthesized in the shape of isometric crystals having octahedron- and cube-shaped faces, with dimensions up to 0.5 cm. They were extracted from the aqueous solution in which they were grown, the surface white opaque stratum was removed, and a paraffin coating was applied. At CityU, luminescence spectra were recorded by a Spex-1403DM spectrometer at a resolution of 2 cm^{-1} using argon-ion laser and mercury arc lamp excitation. In these experiments, the sample was housed in a home-built liquid nitrogen cryostat or an Oxford Instruments Closed Cycle helium cryostat with a base temperature of approximately 10 K. Absorption spectra were recorded at the same resolution using a Biorad FTS-60A spectrometer. Laser-selective excitation and fluorescence spectra were obtained at LBNL using a Spectra Physics PDL-3 dye laser pumped by the third-harmonic output of a Spectra Physics GCR-3 Nd:YAG laser. The dyes Coumarin 500 and Coumarin 460 were used to excite into the $^5D_1$ and $^5D_2$ multiplets of Eu^{3+}, respectively. Emission from the ^5D_J multiplets was analysed at a resolution of approximately 1 cm^{-1} using a Spex 1403 double-grating monochromator and detected by a thermo-electrically cooled Hamamatsu R375 photomultiplier tube, sensitive down to 12 000 cm^{-1}. The signal was amplified by a Stanford Research SR445 fast preamplifier and measured by a SR400 time-gated photon counter. Luminescence transients were recorded using a LeCroy 9360 digital-storage oscilloscope. Experiments were conducted with the sample at room temperature or cooled to 4.2 K using an Oxford Instruments model CF1204 optical cryostat.

3. Results and discussion

3.1. Energy levels

The observed energy levels were fitted using a phenomenological Hamiltonian $H = H_{FI} + H_{\mathrm{CF}}$, employing a simultaneous diagonalization of the free-ion Hamiltonian H_{FI} and the crystal-field Hamiltonian H_{CF}. The free-ion Hamiltonian is given by the expression [1]

$$H_{FI} = \sum_{k=0,2,4,6} F^k(n\mathrm{f}, n\mathrm{f})\, f_k + \zeta_f \alpha_{SO} + \alpha L(L+1) + \beta G(G_2) + \gamma(R_7) + \sum_{k=2,8;k\neq 5} T^k t_k + \sum_{k=0,2,4} M^k m_k + \sum_{k=2,4,6} P^k p_k \quad (1)$$

where the $F^k(n\mathrm{f}, n\mathrm{f})$s and ζ_f represent the radial parts of the electrostatic and spin–orbit interaction, respectively, between f electrons, and f_k and α_{SO} are the angular parts of these interactions. The parameters α, β and γ are associated with the two-body effective operators of the configuration interaction and the T^ks are the corresponding parameters for the three-body configuration interaction. The M^k-parameters arise from spin–spin and spin–other-orbit interactions and the P^k-parameters represent the electrostatic-spin–orbit interaction with higher configurations. The T^k, M^k and P^k are the radial parts of the interactions, whereas the t_k, m_k and p_k are the corresponding angular parts. For the different interaction mechanisms present, the angular parts can be evaluated exactly, while the radial portions

Table 1. Energy levels of Eu^{3+} in Cs_2NaYF_6:EuF_6^{3-} at 4–10 K.

Multiplet term	Crystal-field level	Observed energy[a] (cm^{-1})	Calculated energy (cm^{-1})	Obs. − calc. (cm^{-1})
$^7F_0$	Γ_1	0	9	−9
$^7F_1$	Γ_4	337	359	−22
$^7F_2$	Γ_3	807	792	15
	Γ_5	1065	1085	−20
$^7F_3$	Γ_2	1789	1775	14
	Γ_5	1953	1973	−20
	Γ_4	2014	2023	−9
$^7F_4$	Γ_5	2670	2650	20
	Γ_3	3041	3035	6
	Γ_4	3151	3156	−5
	Γ_1	3205	3224	−19
$^7F_5$	$a\Gamma_4$	3821	3857	−36
	Γ_5	(3881)	3828	53
	Γ_3	(3911)	3884	27
	$b\Gamma_4$	4335	4287	48
$^7F_6$	Γ_3	(4818)	4862	−44
	$a\Gamma_5$	—	4908	—
	Γ_2	—	4989	—
	$b\Gamma_5$	—	5463	—
	Γ_4	—	5497	—
	Γ_1	—	5529	—
$^5D_0$	Γ_1	17 255	17 251	4
$^5D_1$	Γ_4	19 000	18 993	7
$^5D_2$	Γ_5	21 389	21 407	−18
	Γ_3	21 568	21 521	47
$^5D_3$	Γ_5	—	24 306	—
	Γ_4	24 274	24 313	−39
	Γ_2	—	24 350	—

[a] Mean values from table 4—see later. Values in parentheses are uncertain.

are treated as parameters.

For O_h point group symmetry, the CF Hamiltonian can be expressed in terms of two phenomenological parameters B_q^k and the angular tensor operators C_q^k. The values of $|q|$ are limited to 0 and 4 and the Hamiltonian is given [1] by

$$H_{CF} = B_0^4[C_0^4 + \sqrt{(5/14)}(C_{-4}^4 + C_4^4)] + B_0^6[C_0^6 - \sqrt{(7/2)}(C_{-4}^6 + C_4^6)]. \quad (2)$$

The quality of the fits to the above expressions was determined using the deviation σ (in cm^{-1}), which is defined as

$$\sigma = \sum \left[\frac{(E_{exp} - E_{calc})^2}{(N - p)} \right]^{1/2} \quad (3)$$

where N is equal to the number of levels and p is the number of parameters that are varied freely.

Table 2. Energy-level parameters for Eu^{3+} in Cs_2NaYF_6:Eu and Cs_2NaYCl_6:Eu[a].

Parameter	Cs_2NaYF_6:Eu[b]	Cs_2NaYCl_6:Eu[c]
E_{AVE}	64 225(42)	64 226(17)
F^2	83 789(50)	83 902(21)
F^4	[59 909]	[59 990]
F^6	[41 308]	[41 364]
ζ	1323(13)	1324(6)
B_0^4	3138(65)	1928(31)
B_0^6	382(42)	247(22)
N	21	19
σ	31.5	12.2

[a] All values are in cm^{-1}. The parameters are defined in equations (1)–(3). The numbers shown in parentheses are estimates of the uncertainties in the fitted parameter values. The following ratios were held fixed as in [1]: $F^4/F^2 = 0.715$, $F^6/F^2 = 0.493$ (indicated above by square brackets); $M^2/M^0 = 0.56$, $M^4/M^0 = 0.38$; and $P^4/P^2 = 0.75$, $P^6/P^2 = 0.5$. The fixed parameter values $\alpha = 16.8$, $\beta = -640$, $\gamma = 1750$, $T^2 = 370$, $T^3 = 40$, $T^4 = 40$, $T^6 = -330$, $T^7 = 380$, $T^8 = 370$, $M^0 = 2.38$ and $P^2 = 245$ were also the same as in [1].
[b] This study.
[c] From reference [1]; the $^5D_3$ levels included in the fit were taken from the absorption spectrum of $Cs_2NaEuCl_6$.

The energy levels of Eu^{3+} in Cs_2NaYF_6 determined in the present study are summarized in table 1, together with the calculated values. Table 2 lists the derived parameter values and gives the comparison with those from the analysis of the Cs_2NaYCl_6:Eu data-set [1].

3.2. Vibrational spectra

Vibrational spectra have previously been reported for Cs_2KYbF_6 [27], Cs_2KMF_6 (M = Y, La, Gd, Yb) [33] and Cs_2KPrF_6 [34]. The (moiety) normal modes of vibration of MF_6^{3-}, ν_i ($i = 1, 6$), some of which are degenerate, are described by the irreducible representations (irreps) of the O_h molecular point group:

$$\Gamma_{vib} \in S_1, \nu_1(\alpha_{1g}) + S_2, \nu_2(\epsilon_g) + S_4, \nu_5(\tau_{2g}) + S_6, \nu_3; S_7, \nu_4(\tau_{1u}) + S_{10}, \nu_6(\tau_{2u}). \quad (4)$$

Cs_2NaYF_6 belongs to the space group $Fm3m$ (O_h^5), with lattice parameter 0.9056 nm [7], so the Y–F distance is 235 pm. Our vibrational assignments for lanthanide hexafluoroelpasolites are summarized in table 3. The data are taken from the Raman and optical spectra of the present study and from previous studies. No infrared data are available for compounds of the type Cs_2NaMF_6. Recent calculations of vibrational frequencies of octahedral hexafluorometallates, MF_6^{3-}, using second-order Møller–Plesset theory and density functional theory, gave poor data-fits [35]. However, the assignments of the MF_6^{3-} internal modes are consistent with those given here.

The notation S_i (equation (4)) for the ith unit-cell group mode of vibration of the elpasolite lattice is taken from Lentz [36]. In addition to the six moiety modes in (4), the crystal unit cell exhibits another four $\boldsymbol{k} = 0$ modes. Two of these are infrared-active (τ_{1u}) vibrations, comprising motions of the sodium (S_8) and caesium (S_9) nuclei. The other two vibrations are the Raman-active caesium translatory mode ($S_5(\tau_{2g})$) and the Raman- and infrared-inactive rotatory mode ($S_3(\tau_{1g})$).

The Raman spectra of $Cs_2NaY_{1-x}Eu_xF_6$ (figure 1) show the three *gerade* moiety modes

Table 3. Observed energies from vibrational and optical spectra of hexafluoroelpasolites. The normal-mode notation is that of Lentz [36]. S_5, S_8 and S_9 are lattice modes in the unit-cell group analysis. Force-field calculations for the isolated LnF_6^{3-} moiety have been given in reference [40], but are only approximate since the symmetry coordinates of S_7 and S_8 are strongly mixed.

	Observed energy (cm^{-1})								
Compound	$S_1(\nu_1)$	$S_2(\nu_2)$	$S_4(\nu_5)$	S_5	$S_6(\nu_3)$	$S_7(\nu_4)$	S_8	S_9	$S_{10}(\nu_6)$
Cs_2NaYF_6 [a]	472	365	198	69	—	—	—	—	—
Cs_2NaYF_6:Eu[b]	—	—	—	65	373	157	172	55	123
Cs_2KYF_6 [c]	476	382	194	—	400	160	200	80	—
Cs_2KYF_6:Eu[d]	—	—	—	—	372	139	174	—	99
Rb_2NaEuF_6 [e]	—	—	—	—	388	149	—	72	110
Rb_2NaHoF_6 [f]	498	396	205	75	—	—	—	—	—
Cs_2KYbF_6 [a,b]	490	—	194	54	405	153	174	72	115

[a] From 20 K Raman spectra.
[b] 20 K optical spectra of this study. The energies of the τ_{1u} modes refer to transverse optic components; see the text.
[c] From 300 K infrared and Raman spectra [33].
[d] From 100 K optical spectra [25].
[e] From 80 K optical spectra [26].
[f] From 300 K Raman spectra [39].

of Cs_2NaYF_6 together with the τ_{2g} lattice mode, and these are readily assigned by reference to the spectra of $Cs_2NaEuCl_6$ [37]. The intense feature at 415 cm^{-1} below the laser excitation line (figure 1) is the $(^5D_1)\Gamma_4 \rightarrow \Gamma_1(^7F_0)$ zero-phonon line, which becomes stronger relative to the Raman bands with increasing Eu^{3+} concentration. However, its relative intensity does not increase linearly with the number of absorbing centres because concentration quenching of $^5D_1$ emission occurs at this temperature (see section 3.6). The Raman data for $Cs_2NaY_{1-x}Eu_xF_6$ (providing the assignments of $\boldsymbol{k} = 0$ *gerade* modes) reflect the force field of the host lattice Cs_2NaYF_6 in each case, whereas the vibrational energies derived from the optical spectra (providing the assignments of $\boldsymbol{k} = 0$ τ_{1u} *ungerade* modes) depend upon the force field of the EuF_6^{3-} chromophore. Some disparity therefore appears between the energies of the modes of Cs_2NaYF_6 and Cs_2NaYF_6:Eu for example, (table 3), and a complete vibrational data-set is not available in each case.

The G-matrix element for the sodium stretch lattice mode, S_8, is independent of the nature of the halogen coordinated to the Ln^{3+} ion. The F-matrix element does differ however, and the energy of S_8 is between 170 and 180 cm^{-1} for $Cs_2NaLnCl_6$, but near 150 cm^{-1} for $Cs_2NaLnBr_6$. We would therefore expect the energy of S_8 to be somewhat higher for Cs_2NaLnF_6. As mentioned above, no infrared data are available for Cs_2NaLnF_6-type compounds. The energy ratio $\bar{\nu}(S_{8,Na})/\bar{\nu}(S_{8,K})$ for the materials Cs_2ALnX_6 (A = Na, K) is calculated from the G-matrix element to be 1.25. The infrared spectra of Cs_2KMF_6 exhibit two strong overlapping bands between 140 and 200 cm^{-1} [33]. Thus the lower-energy band (table 3) might correspond to predominantly internal-mode character. The bending modes ν_4, ν_5 and ν_6 show an energy decrease with increasing ionic radius of A^+ for Cs_2AEuCl_6 [37], and this behaviour should also be apparent for Cs_2ALnF_6 (table 3: Cs_2NaYF_6:Eu and Cs_2KYF_6:Eu). From the optical spectra of Cs_2NaYF_6:Eu in the present study, the most intense feature between 150 and 200 cm^{-1} is at 157 cm^{-1} and is clearly of predominantly $S_7(\nu_4)$ character. A very weak band near 172 cm^{-1} is assigned to

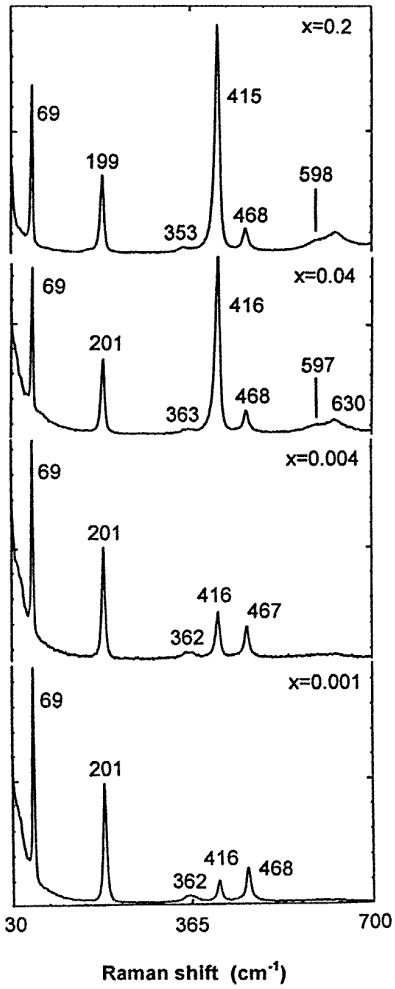

Figure 1. 514.5 nm excited 300 K Raman spectra of $Cs_2NaY_{1-x}Eu_xF_6$. The emission bands which appear at higher Eu^{3+} concentrations are due to the $(^5D_1)\Gamma_4 \rightarrow \Gamma_1(^7F_0)$ zero-phonon line (located at the Raman shift 415 cm^{-1}), and the $(^5D_1)\Gamma_4 + S_7, S_{10} \rightarrow \Gamma_4(^7F_1)$ vibronic structure (at 597, 630 cm^{-1}).

S_8. We stress, however, that there is extensive mixing of τ_{1u}-symmetry coordinates for the $S_7(\nu_4)$ moiety mode and the S_8 lattice mode, with reference to the assignments given for the S_8 and S_7 modes in Cs_2AMF_6 (table 3).

Lattice dynamics calculations have been performed for several hexafluoroelpasolite crystals on the basis of fits to $\boldsymbol{k} = 0$ Raman modes [38]. The modelling of *ungerade* modes was not accurate however, because eight non-zero-energy τ_{1u} modes were predicted at the zone centre for K_2NaMF_6 (M = Sc, Ga).

3.3. Absorption and excitation spectra

We were unable to observe the weak vibronic sidebands of the f–f electronic *absorption* transitions of Eu^{3+} in the dilute crystals Cs_2NaYF_6:Eu. Several MD zero-phonon lines

Table 4. Zero-phonon lines in the absorption, excitation and emission spectra of Eu^{3+}-doped Cs_2NaYF_6. abs: absorption spectra; exc: excitation spectra. The energies of origins inferred from vibronic structure are given, but those given in bold type were (also) directly observed zero-phonon lines. Where different, the inferred locations of the terminal energy levels are listed underneath the electronic origin energies in each case (in italics). The energies are different for the 0.1%- and 20%-Eu-doped crystals partly because of the different crystalline field and site symmetry experienced by Eu^{3+} due to temperature and concentration changes, and also because of experimental factors such as calibration uncertainties.

		20%-doped Cs_2NaYF_6: 10 K spectra				0.1%-doped Cs_2NaYF_6: 4 K spectra		
Terminal level		abs or exc	Emission from			Emission from		
			$^5D_2$	$^5D_1$	$^5D_0$	$^5D_3$	$^5D_1$	$^5D_0$
$^7F_0$	Γ_1	0	0	0	0	0	0	0
$^7F_1$	Γ_4	—	—	**18 663**	**16 914**	—	**18 670**	**16 918**
				337	*341*		*334*	*337*
$^7F_2$	Γ_3	—	—	**18 193**	16 445	—	**18 201**	16 448
				807	*810*		*803*	*807*
	Γ_5	—	—	**17 954**	16 193	—	**17 940**	16 186
				1066	*1062*		*1064*	*1069*
$^7F_3$	Γ_2	—	**19 600**	—	—	—	—	—
			1789					
	Γ_5	—	**19 434**	**17 047**	15 304	—	**17 049**	15 303
			1955	*1953*	*1951*		*1955*	*1952*
	Γ_4	—	**19 369**	—	**15 245**	—	**16 989**	**15 244**
			2020		*2010*		*2015*	*2011*
$^7F_4$	Γ_5	—	**18 716**	—	14 588	**21 606**	**16 331**	14 584
			2673		*2667*	*2668*	*2673*	*2671*
	Γ_3	—	—	**15 961**	14 216	**21 234**	**15 959**	14 213
				3039	*3039*	*3040*	*3045*	*3042*
	Γ_4	**3150**[a]	—	15 852	**14 104**	**21 124**	15 849	**14 103**
				3148	*3151*	*3150*	*3155*	*3152*
	Γ_1	—	—	**15 797**	14 051	**21 070**	**15 795**	14 051
				3203	*3204*	*3204*	*3209*	*3204*
$^7F_5$	$a\Gamma_4$	—	—	**15 180**	13 437	—	**15 179**	—
				3820	*3818*		*3825*	
	Γ_5	—	—	—	—	—	(15 123)	—
							(3881)	
	Γ_3	—	—	—	—	—	(15 093)	—
							(3911)	
	$b\Gamma_4$	—	—	—	**12 922**	—	14 665	**12 922**
					4333		*4339*	*4333*
$^7F_6$	Γ_3	—	—	(14 182)	—	—	—	—
				(4818)				
$^5D_0$	Γ_1	—	—	—	17 255	—	—	17 255
$^5D_1$	Γ_4	**18 999**	**19 000**			—	—	—
$^5D_2$	Γ_5	21 389	21 389	—		—	—	—
	Γ_3	21 568	—	—		—	—	—
$^5D_3$	Γ_4	**24 274**	—	—		24 274	—	—

[a] At 100 K.

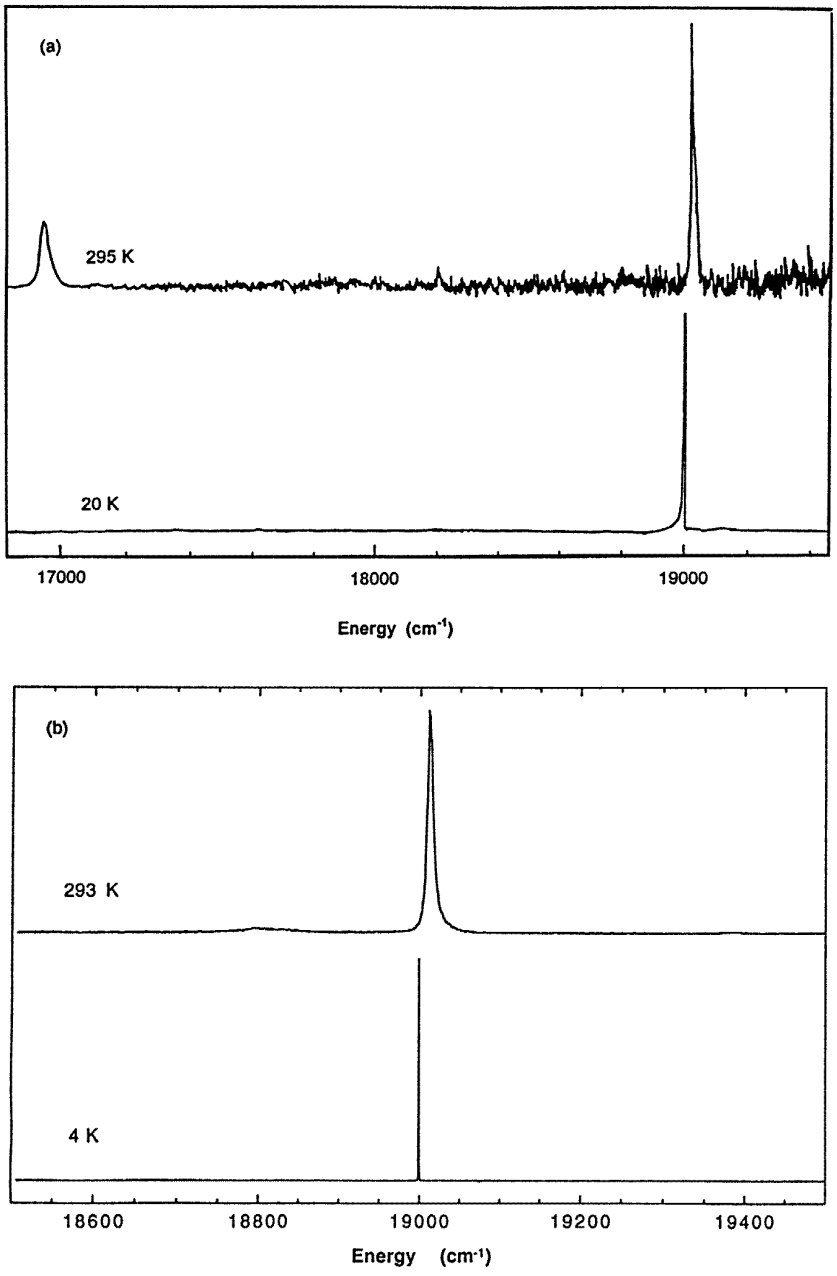

Figure 2. Visible absorption (a) and excitation (b) spectra of Cs_2NaYF_6:Eu. $Cs_2NaY_{0.8}Eu_{0.2}F_6$ was used for the absorption spectra. The $^5D_0$ emission at 16 917 cm^{-1} was monitored in the excitation spectra of $Cs_2NaY_{0.999}Eu_{0.001}F_6$.

(ZPL) were however located from the infrared and visible absorption spectra, and the derived energy levels are summarized in table 4. Figure 2(a) shows that the $(^7F_0)\Gamma_1 \rightarrow \Gamma_4(^5D_1)$ transition shifts to a lower energy on cooling from 295 K to 20 K (refer to section 3.5 for a more detailed discussion). The excitation spectra within a narrower region are shown in

figure 2(b) for the 0.1%-Eu-doped crystal. The hot bands in the room temperature spectrum enable the identification of thermally populated ^7F_J ($J = 1, 2$) levels. For example, the features at 16 913 cm^{-1} and 18 190 cm^{-1} in figure 2(a) correspond to the $(^7F_1)\Gamma_4 \rightarrow \Gamma_1(^5D_0)$ and $(^7F_2)\Gamma_3 \rightarrow \Gamma_4(^5D_1)$ zero-phonon lines respectively.

With the exception of MD and EQ ZPL, the electronic spectra of lanthanide elpasolites are essentially vibronic in nature, with the strongest intensity generally arising from the $S_6(\nu_3)$, $S_7(\nu_4)$ and $S_{10}(\nu_6)$ odd-parity internal modes. The relative intensities of these vibronic origins may vary enormously from one transition to another, and simple vibronic intensity point group selection rules may be effective in restricting the intensity in some transitions—such as the absence of τ_{1u} modes in Γ_1–Γ_2 transitions, and the absence of the τ_{2u} mode in Γ_1–Γ_1 transitions. More subtle effects such as the mixing of vibrations, the occurrence of transverse mode–longitudinal mode (TO–LO) splittings, and deviations from $\boldsymbol{k} = 0$ selection rules, lead to the occurrence of multiple structure for each vibronic origin, and the presence of lattice modes in the electronic spectra.

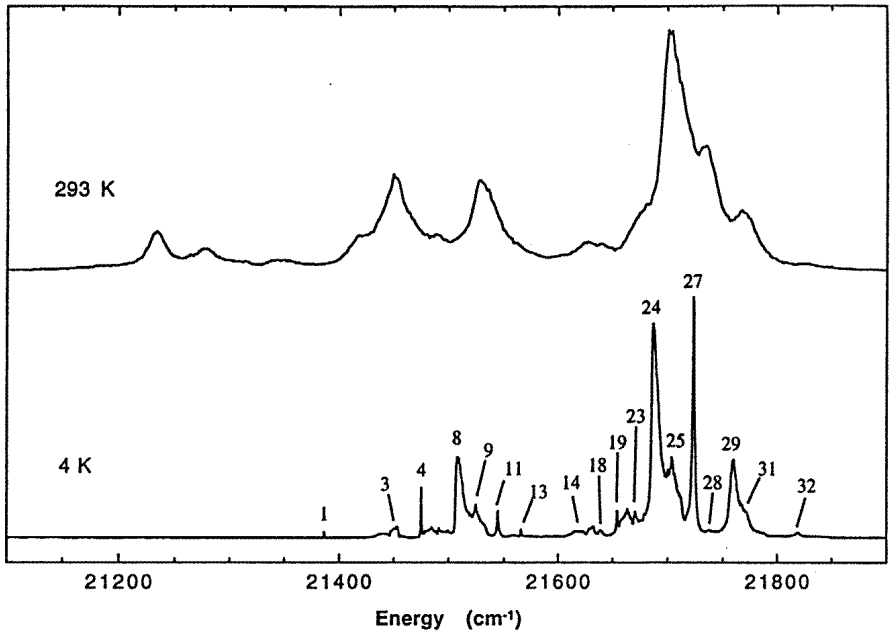

Figure 3. Excitation spectra of the $^7F_0 \rightarrow {}^5D_2$ transitions in $Cs_2NaY_{0.999}Eu_{0.001}F_6$. The $^5D_1$ emission at 18 194 cm^{-1} was monitored.

The $(^7F_0)\Gamma_1 \rightarrow \Gamma_5, \Gamma_3(^5D_2)$ excitation spectrum (figure 3) provides the opportunity to study the vibronic structure of two transitions of Cs_2NaYF_6:Eu where overlapping does not lead to ambiguities of interpretation. Assignments are collected together in table 5. In $Cs_2NaEuCl_6$, the strongest vibronic origin of each of these $\Gamma_1 \rightarrow \Gamma_5, \Gamma_3$ transitions is ν_6, with that of the $\Gamma_1 \rightarrow \Gamma_5$ transition being more intense. The same trend is observed for Cs_2NaYF_6:Eu, where the maximum of ν_6 is at 123 cm^{-1} at 4 K. It has been pointed out that this maximum may not correspond to the zone-centre mode [41]. The comparison also enables the maximum intensity from ν_4 to be assigned at 157 cm^{-1} and that from ν_3 to be assigned at 373 cm^{-1} (table 5). The *vibrational* energies exhibit changes with temperature: on cooling from 300 K to 4 K, that of ν_3 increases by $\sim$6 cm^{-1} whilst that of ν_6 decreases

Table 5. Assignments of the $(^7F_0) \rightarrow \Gamma_3, \Gamma_5(^5D_2)$ vibronic sidebands of Cs_2NaYF_6:Eu. The numbered bands are described in terms of their widths and intensities: w: weak; m: medium; s: strong; v: very; sh: shoulder; b: broad; nr: not recorded.

Line, figure 3	$(^7F_0) \rightarrow \Gamma_5(^5D_2)$ line position[a] (cm^{-1})	Line, figure 3	$(^7F_0) \rightarrow \Gamma_3(^5D_2)$ line position[a] (cm^{-1})	Assignment[b]
1w	21 386	13w	21 566	Zero-phonon line
2bw	55	14bw	51	S_9
		15bw	57	
3w	65	16w	63	S_5
		17w	66	
		18w	73	
4m	89	19mw	88	
		20w	92	
5vw	98	21w	97	
6vw	105	22w	104	
7vw	113	23w	113	
8ms	123	24s	123	S_{10}, ν_6
9m	138	25ms	138	
10sh	146	26sh	146	
11mw	158	27s	157	S_7, ν_4
12vw	172	28vw	171	S_8
29ms	373		nr	S_6, ν_3
(30)sh	381			S_2, ν_2 ZB
31sh	385			
32vw	(432)	32vw	(252)	

[a] Except for the zero-phonon line, the columns represent the difference between the zero-phonon line and the vibronic peaks.

[b] The labelling of vibrations follows [36] and is given in table 3 and equation (4). Only maxima associated with unit-cell group modes are indicated. Dispersion and guest–host coupling of vibrations need to be considered for more detailed assignments (section 3.3).

by $\sim$4 cm^{-1}. Other fine structure is observed in figure 3. The Eu concentration in the crystal was 0.1%, but clustering of ions could lead to the dispersion of the wavevector at different points in the reciprocal lattice. From previous studies [41–43], the bands between 50 and 70 cm^{-1} correspond to Cs^+ motion and those between 90 and 113 cm^{-1} correspond to F^- motion and two-phonon modes. The coupling of guest modes to those of the host which are slightly higher in energy has been observed for the Cs_2NaYCl_6 lattice [44], and the higher-energy structure at 8–15 cm^{-1} above ν_6 and ν_3 in the present spectra could be similarly assigned. The bands are labelled in table 5 according to the $\boldsymbol{k} = 0$ parentage of the unit-cell group modes, and we do not provide more detailed assignments at this stage. From the room temperature infrared spectra of Cs_2KLnF_6, the TO–LO splitting of ν_3 appears to be about 35 cm^{-1} [33], but the LO modes are not apparent in the optical spectra of the diluted crystals in the present study. Finally, a shoulder is observed at 25 cm^{-1} below several intense MD ZPL in emission, and this presumably corresponds to a zone-boundary acoustic mode.

Figure 3 also shows the extensive broadening of vibronic structure in the excitation spectrum which accompanies increases in temperature. The new hot bands which are observed can be assigned to absorption from thermally populated vibronic and electronic levels of the $(^7F_0)\Gamma_1$ ground state and $(^7F_1)\Gamma_4$ excited state. The derived energy of $(^7F_1)\Gamma_4$ is 349 cm^{-1} at room temperature.

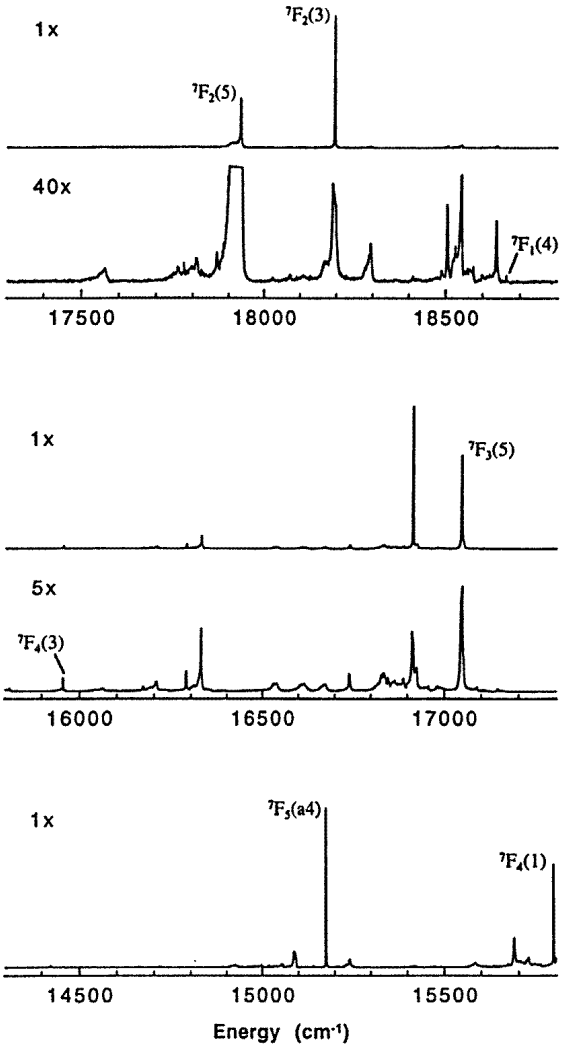

Figure 4. 4 K emission spectra of $Cs_2NaY_{0.999}Eu_{0.001}F_6$ recorded with laser excitation at 19 000 cm^{-1}. A time gate open from 10 μs to 1 ms after the laser pulse was used to select the $^5D_1$ multiplet emission. The transitions are labelled by their terminal levels, with the O_h point group irrep labels given in brackets.

3.4. Assignment of luminescence spectra

The features in the vibrational sidebands of the two electronic transitions in table 5 have very similar displacements from the respective ZPL. We have utilized this fine-structure vibrational fingerprint to locate the (unobserved) electronic origins of other transitions in the emission spectra of Cs_2NaYF_6:Eu. The emission spectra of the 0.1%- and 20%-Eu-doped materials were very similar, except for the different relative intensities of transitions originating from different multiplets. Splittings of MD ZPL of up to 4 cm^{-1} were observed in the emission spectra of the 20%-Eu-doped crystals, but not for the 0.1%-Eu-doped material. This indicates a slight distortion from the ideal octahedral site symmetry in the more highly

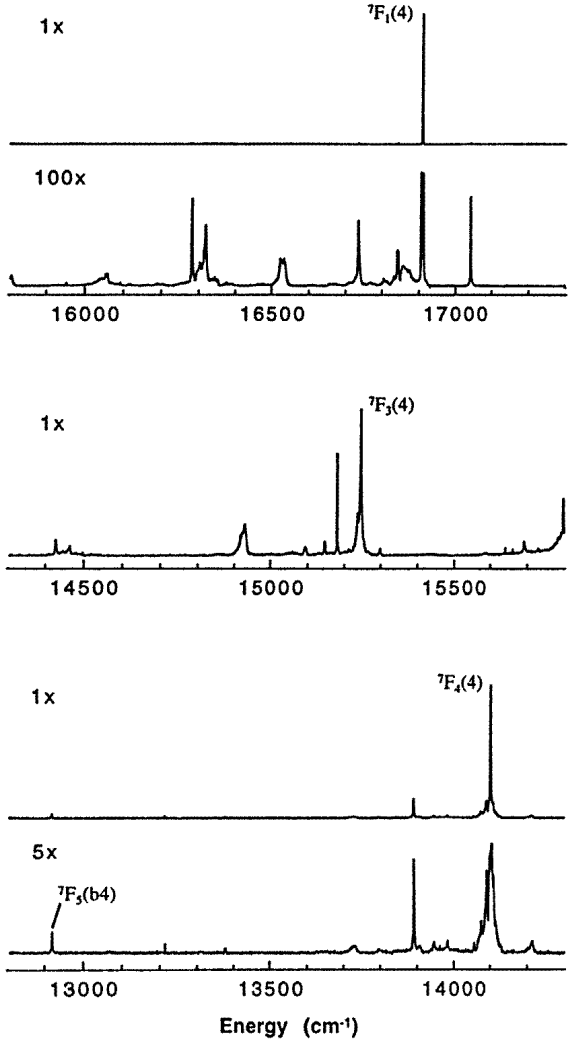

Figure 5. 4 K emission spectra of $Cs_2NaY_{0.999}Eu_{0.001}F_6$ recorded with laser excitation at 19 000 cm^{-1}. A time gate open from 500 μs to 10 ms after the laser pulse was used to select the $^5D_0$ multiplet emission. The transitions are labelled by their terminal levels, with the O_h point group irrep labels given in brackets.

doped crystals.

Emission was observed from the ^5D_J ($J = 0, 1, 2, 3$) multiplets of Eu^{3+}, and selective-excitation experiments together with temporal gating of the emission enabled the emitting levels to be determined. The survey spectrum in figure 4 shows the emission from $^5D_1$ at short gate-delay times, whereas that from $^5D_0$ dominates at longer times (figure 5). The broadening of spectral features with increasing temperature is evident in figure 6. The high vibrational frequencies of the EuF_6^{3-} moiety lead to weak anti-Stokes emission hot bands in the spectra of EuF_6^{3-}, compared with the spectra of $EuCl_6^{3-}$. In general the luminescence spectra of EuF_6^{3-} are not as clearly resolved as the corresponding spectra of $EuCl_6^{3-}$, but the detailed interpretation of the latter spectra together with the analysis of the complete set of

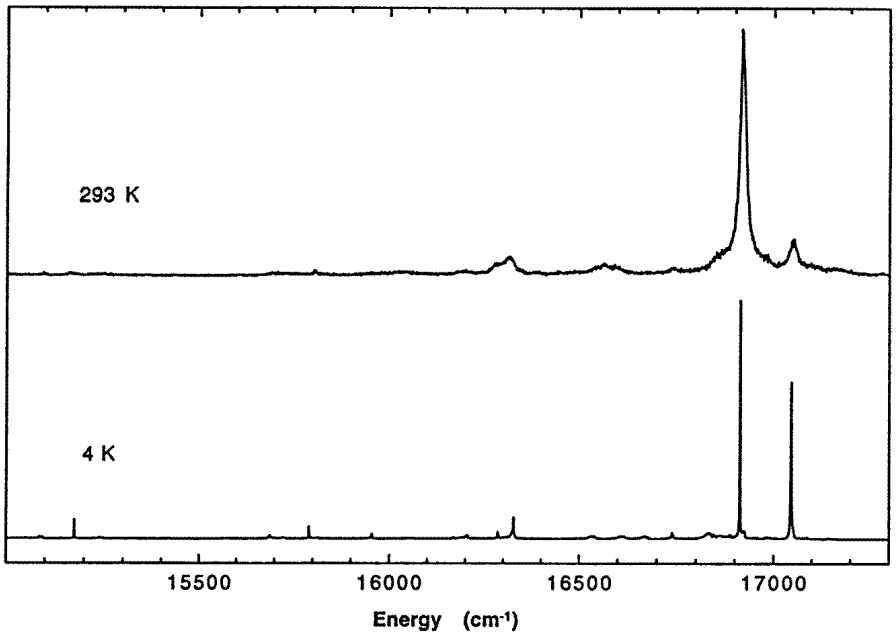

Figure 6. 293 K and 4 K emission spectra of $Cs_2NaY_{0.999}Eu_{0.001}F_6$ recorded with laser excitation into the $^5D_1$ multiplet with a time gate open from 10 μs to 1 ms after the laser pulse.

emission, excitation and absorption data for EuF_6^{3-} have enabled all bands to be assigned for EuF_6^{3-}. The vibronic analyses of EuF_6^{3-} follow the same fingerprint pattern as in table 5, so detailed tabulations are not included herein, but the main points in the assignments are now briefly discussed. The results from the spectral analyses, including the listing of observed (and inferred) electronic origins and the derived energies of the ^7F_J and ^5D_J crystal-field levels, are summarized in table 4.

3.4.1. Emission from $^5D_3$. Under 24 712 cm^{-1} Hg-lamp excitation, four lines were observed between 21 606 and 21 070 cm^{-1} in 0.1%-Eu-doped Cs_2NaYF_6 which correspond to the ($\Delta J = 1$) magnetic-dipole-allowed ZPL of transitions terminating on the levels of $^7F_4$ (table 4). Emission to higher-multiplet terms was too weak to be observed, and/or masked by other ^5D_J ($J = 2, 1, 0$) structure.

3.4.2. Emission from $^5D_2$. A major difference between the luminescence of Cs_2NaYCl_6:Eu [45] and Cs_2NaYF_6:Eu is the much weaker intensity of emission from $^5D_2$ under direct excitation into this level for the latter compound (see section 3.6). For Cs_2NaYCl_6:Eu, the strongest $^5D_2$ transitions are the MD ZPL of $^5D_2 \rightarrow {}^7F_3$, and the observed and calculated intensities are in agreement [45]. At 293 K, pumping at 21 793 cm^{-1} in 0.1%-doped Cs_2NaYF_6:Eu, an (unobserved) ZPL is inferred to be at 20 582 cm^{-1} from the $\pm\nu_6$ vibronic structure. Taking the $(^7F_2)\Gamma_3$ energy from the 300 K absorption and emission spectra (823 ± 2 cm^{-1}), $(^5D_2)\Gamma_5$ is inferred to be at 21 403 cm^{-1} at this temperature. A sharper band is located 1091 cm^{-1} below $(^5D_2)\Gamma_5$ (i.e. at 20 312 cm^{-1}), and corresponds to the

$(^5D_2)\Gamma_5 \rightarrow \Gamma_5(^7F_2)$ ZPL. Four lines between 19 606 and 19 382 cm^{-1} are assigned to $(^5D_2)\Gamma_3, \Gamma_5 \rightarrow \Gamma_2, \Gamma_5, \Gamma_4(^7F_3)$, with the terminal levels derived to be at 1797 cm^{-1} (Γ_2), 1961 cm^{-1} (Γ_5) and 2021 cm^{-1} (Γ_4). Below 20 K, under a Xe lamp, Hg 404 nm, or argon-ion 476.5 nm excitation, weak features are observed in this region in Cs_2NaYF_6:Eu at 19 600, 19 433 and 19 369 cm^{-1}, which are identified with the $(^5D_2)\Gamma_5 \rightarrow \Gamma_2, \Gamma_5, \Gamma_4(^7F_3)$ zero-phonon emission lines. The strongest MD transition to $^7F_4$ (to the Γ_5 terminal level) is also observed very weakly.

3.4.3. Emission from $^5D_1$. At 10 K, emission from $(^5D_1)\Gamma_4$ was obtained by pumping the $\Gamma_1(^7F_0) \rightarrow (^5D_1)\Gamma_4$ ZPL of $Cs_2NaY_{0.8}Eu_{0.2}F_6$ at 19 000 $\pm$ 2 cm^{-1}. The spectrum is dominated by some intense MD-allowed ZPL to levels at 807 cm^{-1} ($(^7F_2)\Gamma_3$), 1066 cm^{-1} ($(^7F_2)\Gamma_5$), and 1953 cm^{-1} ($(^7F_3)\Gamma_5$). Weak ν_3, ν_4 and ν_6 vibronic origins enable the location of the $(^5D_1)\Gamma_4 \rightarrow \Gamma_4(^7F_1)$ origin at 18 663 cm^{-1} to be established, so $\Gamma_4(^7F_1)$ is located at 337 cm^{-1}. The complex group of bands between 16 500 and 17 200 cm^{-1} was observed at 4 K in Cs_2NaYF_6 doped with 0.1% Eu using a short gate time, from 10 μs to 1 ms (figure 4). Under these conditions the $^5D_1$ emission appeared more intense, and a further electronic origin was located from extensive vibronic structure, at 16 989 cm^{-1}, corresponding to $(^5D_1)\Gamma_4 \rightarrow \Gamma_4(^7F_3)$. The vibronic sideband of the transition to the terminal $(^7F_3)\Gamma_2$ level is overlapped by other structure. Under the same time gate, the vibronic sideband of $(^5D_1)\Gamma_4 \rightarrow \Gamma_5(^7F_4)$ is clearly located, with the origin inferred to be at 16 331 cm^{-1} at 8 K in the 0.1%-doped material. The transition to $\Gamma_3(^7F_4)$ is also clearly observed, with the ZPL at 15 959 cm^{-1} at 4 K. The $\Gamma_4(^7F_4)$ terminal level is located from its associated ν_4 and ν_6 structure. The remaining ($^7F_4$) CF level, Γ_1 (15 795 cm^{-1} at 4 K), is located from the intense ZPL, very weak ν_4, ν_6 structure, and a medium-intensity ν_3 band.

As in the emission of $Cs_2NaEuCl_6$, the $(^5D_1)\Gamma_4 \rightarrow a\Gamma_4(^7F_5)$ MD ZPL is relatively intense, being located at 15 179 cm^{-1} at 4 K. The highest ($^7F_5$) CF level is assigned at 4339 cm^{-1}, from the $(^5D_1)\Gamma_4 \rightarrow b\Gamma_4(^7F_5) + \nu_6, \nu_4$ vibronic origins, as in $Cs_2NaEuCl_6$. Two weak features in the short-time-gate spectrum remain unassigned. The first is most reasonably assigned to a ν_3 vibronic origin, and the second to ν_4. The derived energies of the terminal states are then $(^7F_5)\Gamma_5$ at 3881 cm^{-1} and $(^7F_5)\Gamma_3$ at 3911 cm^{-1}. These two states are transposed as compared to the calculated energy-level scheme for $Cs_2NaEuCl_6$. The spectral data from the present study do not unambiguously permit the assignment of irreps to energy levels in these cases, and this transposition of irrep assignments gave the best fit to the two measured energy levels. The $(^5D_1)\Gamma_4 \rightarrow {}^7F_6$ group is obscured by the $^5D_0 \rightarrow {}^7F_4$ group, but bands at 13 807, 14 060 and 14 042 cm^{-1} in the short-time-gate spectrum of the 20%-Eu-doped material may be associated with an unobserved origin at 14 182 cm^{-1}, although overlapping occurs with some strong bands in the long-time-gate spectrum. The terminal state is then calculated to be at 4818 cm^{-1}, and is assigned to the lowest $^7F_6$ level, Γ_3.

3.4.4. Emission from $^5D_0$. In $Cs_2NaY_{0.8}Eu_{0.2}F_6$ the intense $(^5D_0)\Gamma_1 \rightarrow \Gamma_4(^7F_1)$ ZPL is observed at 16 921 cm^{-1} at 295 K, and is split into two components at 16 912 and 16 916 cm^{-1} by a tetragonal (or lower-symmetry) perturbation at 17 K. No splitting was resolved at 4 K in Cs_2NaYF_6 doped with 0.1% Eu, and the ZPL is located at 16 918 cm^{-1} (refer to figures 2(b) and 5). Only two associated vibronic origins are located: S_8 at 179 cm^{-1} and $\nu_3(S_6)$ at 383 cm^{-1} below the electronic origin. These energies are higher than for other electronic transitions, and the intensity of S_8 is relatively large, as for the $(^7F_0)\Gamma_1 \rightarrow \Gamma_1(^5D_0)$ absorption transition of $Cs_2NaEuCl_6$ [30]. The $(^5D_0)\Gamma_1 \rightarrow \Gamma_1(^7F_0)$

transition is too weak to be observed, and the electronic origin is inferred to be at 17 255 cm^{-1} in $Cs_2NaY_{0.8}Eu_{0.2}F_6$ from the location of other $(^5D_0)\Gamma_1 \rightarrow {}^7F_J$ transitions. The ZPL of the $(^5D_0)\Gamma_1 \rightarrow \Gamma_3(^7F_2)$ transition is also not observed, but is located from ν_3, ν_4, ν_6 and lattice mode structure. The $(^5D_0)\Gamma_1 \rightarrow \Gamma_5(^7F_2)$ origin is located from the prominent ν_3 vibronic structure, but the lower part of the vibronic sideband of this transition is obscured. The $(^5D_0)\Gamma_1 \rightarrow {}^7F_3$ group of bands is marked by an intense ZPL ($\Gamma_1 \rightarrow \Gamma_4(^7F_3)$) at 15 245 cm^{-1}, and ν_3, ν_4 and ν_6 vibronic origins based upon $\Gamma_1 \rightarrow \Gamma_5(^7F_3)$. The transitions to $^7F_4$ are observed below 14 590 cm^{-1}. The only MD-allowed transition, $(^5D_0)\Gamma_1 \rightarrow \Gamma_4(^7F_4)$, is observed as an intense ZPL at 14 104 cm^{-1}. Weak ν_3, ν_4 and ν_6 vibronic origins associated with this transition are located to lower energy. To higher energy, two complete, well-resolved vibronic sidebands enable the (unobserved) $(^5D_0)\Gamma_1 \rightarrow \Gamma_3, \Gamma_5(^7F_4)$ origins to be inferred at 14 216 and 14 588 cm^{-1} respectively at 10 K in the 20%-Eu-doped material. The remaining $(^5D_0)\Gamma_1 \rightarrow {}^7F_4$ transition to the terminal Γ_1 level is expected to exhibit the characteristic τ_{1u} vibronic sideband. Only one medium-intensity feature is observed and this is assigned to the ν_4 vibronic origin. By analogy with the spectrum of $Cs_2NaEuCl_6$, the strong sharp feature in the $(^5D_0)\Gamma_1 \rightarrow {}^7F_5$ region is assigned to the transition to the terminal $b\Gamma_4$ level. A weaker sharp band is coincident with the expected position of $\Gamma_1 \rightarrow \Gamma_3$, but is too intense to correspond to this EQ-allowed origin. The $(^5D_0)\Gamma_1 \rightarrow a\Gamma_4(^7F_5)$ origin is not observed, but is inferred to be at 13 437 cm^{-1} from the ν_6, ν_3 sideband.

3.5. Temperature shifts of energy levels

The temperature shifts of CF levels in Cs_2NaYF_6:Eu are appreciable, and those of the 11 levels in table 6 are all negative, whereas those for the levels of Cs_2UX_6 are nearly all positive. Also included in the table are the calculated energy-level shifts from the parametrizations of the 11-level data-sets at 295 K and 4–10 K. The values are in reasonable agreement with experiment. With such sparse data-sets, the uncertainties in the parameter values are high, but the values listed in the table do indicate a larger crystal-field strength at low temperature. The fourth- and sixth-order crystalline-field parameters for U^{4+} in Cs_2UCl_6 are about 3.5 times larger than for Eu^{3+} in Cs_2NaYF_6. Whereas the changes in these parameters with temperature dominate the (positive) temperature shifts in Cs_2UCl_6, clearly other factors play a role in the temperature shifts of energy levels for the case of Eu^{3+} in Cs_2NaYF_6. The Slater parameter F^2 is roughly double the value found for U^{4+} in Cs_2UCl_6, and might be expected to play a more important role in the Eu^{3+} temperature shifts. In fact the parameter F^2 is calculated from the parametrizations of the 11-level data-sets (with great uncertainty) to be smaller at low temperature than at high temperature for Eu^{3+} in Cs_2NaYF_6 (table 6). This is consistent with the reduction in Slater parameters on going from the free ion to the crystalline environment, known as the nephelauxetic effect and attributed to f-electron covalency, although Newman has given an alternative explanation in terms of ligand polarizability (discussed in reference [46]).

Also included in table 6 are the shifts of the corresponding energy levels, as measured at low temperature, between Cs_2NaYCl_6:Eu and Cs_2NaYF_6:Eu, labelled as ΔE(Cl–F), Obs. The shifts of lower levels are positive, but those of the higher energy levels are negative. The calculated energy-level shifts, ΔE(Cl–F), Calc., as deduced from the 19-level fit for Cs_2NaYCl_6:Eu [1] and the 21-level fit for Cs_2NaYF_6:Eu, are in reasonable agreement with experiment. From the chloro- to the fluoro-compound there is a large increase in the CF parameters, but the comparison of the other parameters is beset by their large uncertainties. The parametrizations of the much larger data-sets in reference [28] showed a small increase

Table 6. Observed shifts of energy levels in Cs_2NaYF_6:Eu with temperature and shifts from Cs_2NaYCl_6:Eu to Cs_2NaYF_6:Eu. (In all cases the parameters not detailed in the footnotes were constrained to the values given in table 2.)

		Energy at 295 K		Energy at 4–10 K		$\Delta E(T)$[a]		ΔE(Cl–F)[b]	
Term	Crystal-field level	Obs. (cm^{-1})	Calc.[c] (cm^{-1})	Obs. (cm^{-1})	Calc.[d] (cm^{-1})	Obs. (cm^{-1})	Calc. (cm^{-1})	Obs. (cm^{-1})	Calc.[e] (cm^{-1})
$^7F_0$	Γ_1	0	5	0	−3	—	—	—	—
$^7F_1$	Γ_4	349	360	337	349	−12	−11	22	14
$^7F_2$	Γ_3	823	807	807	788	−16	−19	65	80
	Γ_5	1091	1092	1065	1077	−26	−15	21	18
$^7F_3$	Γ_2	1797	1791	1789	1780	−8	−11	18	24
	Γ_5	1961	1964	1953	1955	−8	−9	−55	−46
	Γ_4	2021	2022	2014	2019	−7	−3	−50	−55
$^5D_0$	Γ_1	17 262	17 259	17 255	17 252	−7	−7	−49	−45
$^5D_1$	Γ_4	19 013	19 011	19 000	19 002	−13	−9	−39	−46
$^5D_2$	Γ_5	21 403	21 439	21 389	21 424	−14	−15	−8	−29
	Γ_3	21 576	21 545	21 568	21 534	−8	−11	−73	−70

[a] $\Delta E(T)$, Obs. is the measured shift, *relative to the electronic ground state*, from 4–10 K to 295 K (i.e. E(4–10 K) − E(295 K)) for the relevant energy level in Cs_2NaYF_6:Eu. $\Delta E(T)$, Calc. is the difference in energy for the given energy level between parametrizations of the 4–10 K and 295 K data-sets.

[b] The shift from Cs_2NaYCl_6:Eu to Cs_2NaYF_6:Eu for the relevant energy level, measured at 4–20 K.

[c] An 11-level fit, with rounded free-parameter values, with standard deviations in parentheses: E_{AVE} = 64 339(36); F^2 = 83 953(43); ζ = 1328(11); B_0^4 = 2887(68); B_0^6 = 425(74).

[d] A fit to the same 11 levels as in footnote c: E_{AVE} = 64 320(40); F^2 = 83 930(48); ζ = 1327(12); B_0^4 = 2981(74); B_0^6 = 523(81).

[e] For Cs_2NaYF_6:Eu, a 21-level fit with the parameters given in table 2. For Cs_2NaYCl_6:Eu, a 19-level fit with the parameters given in table 2.

in the Slater parameter F^2 from the Tb^{3+} chloro- to the fluoroelpasolite, as expected from the decreasing ligand polarizability, but the uncertainties in the spin–orbit parameter values were larger than the differences.

3.6. Luminescence decay kinetics

For Cs_2NaYF_6:Eu, emission was observed from both $^5D_1$ and $^5D_0$ when pumping $^5D_1$, and from ^5D_J ($J = 0, 1, 2$) when pumping $^5D_2$. The emission spectra of the samples containing 0.1% and 20% Eu were very similar, *except* that transitions originating from the three different luminescent levels had different relative intensities. As noted above, the emission from $^5D_2$ is very weak, and *much* weaker than for Cs_2NaYCl_6:Eu. At room temperature, upon excitation into the upper level in each case, the emission from $^5D_{J+1}$ is stronger (relative to that from ^5D_J, $J = 0, 1$) in 0.1%- *than in* 20%-Eu-doped Cs_2NaYF_6:Eu. For Cs_2NaYF_6:Eu the phonon-assisted cross-relaxation process

$$(^5D_2)\Gamma_5 + (^7F_0)\Gamma_1 \rightarrow (^5D_1)\Gamma_4 + (^7F_3)\Gamma_4 + \text{phonon(s)}$$

can occur with the energy mismatch accommodated by one ($\nu_2 \sim 375$ cm^{-1}) or more phonons. The rise time of the $^5D_1$ emission has been found experimentally to be the same as the $^5D_2$ decay time (table 7), supporting this mechanism. In the case of Cs_2NaYCl_6:Eu, the energy mismatch (459 cm^{-1}) is greater than the maximum single-phonon energy.

Table 7. Luminescence rise and decay times (in ms) for multiplets of Eu^{3+} in $Cs_2NaY_{1-x}Eu_xF_6$.

	$x = 0.001$		$x = 0.20$	
Measurement	$T = 295$ K	$T = 4$ K	$T = 295$ K	$T = 4$ K
$^5D_2$ decay time[b]	—	0.084 ± 0.004	—	0.049 ± 0.003
$^5D_1$ rise time[b]	—	0.082 ± 0.004	—	0.048 ± 0.003
$^5D_1$ decay time[b]	—	2.6 ± 0.1	—	2.5 ± 0.1
$^5D_1$ decay time[a]	1.24 ± 0.05	2.7 ± 0.1	0.22 ± 0.01	2.5 ± 0.1
$^5D_0$ rise time[a]	1.18 ± 0.05	3.8 ± 0.2	0.21 ± 0.01	3.4 ± 0.2
$^5D_0$ decay time[a]	15 ± 1	15 ± 1	13 ± 1	15 ± 1

[a] With excitation into the $^5D_1$ multiplet. The same $^5D_0$ decay times were measured for direct $^5D_0$ excitation.
[b] With excitation into the $^5D_2$ multiplet.

We have made a preliminary study of the $^5D_1$ and $^5D_0$ decay kinetics in Cs_2NaYF_6:Eu. The luminescence decay curves were fitted to appropriate single- or double-exponential functions, and the results are summarized in table 7. The (e^{-1}) decay time of $^5D_0$ is independent of temperature and Eu^{3+} concentration, showing the minor importance of defect site processes in depopulating this level. Defect sites are however known to occur in our crystals, because the room temperature infrared spectrum shows a feature near 3600 cm^{-1}. This feature splits into two doublets at 100 K (3667, 3661 cm^{-1} and 3647, 3641 cm^{-1}), and the absence of a prominent band near 1600 cm^{-1} may indicate the presence of hydroxo-complexes.

The $^5D_1$ lifetime is similar in the 20%- and 0.1%-doped crystals at 4 K, but shows a decrease with increasing temperature, more markedly for the more concentrated crystals, so a thermally activated quenching process is operative. The $^5D_1$–$^5D_0$ energy gap is similar in $Cs_2NaEuCl_6$ and Cs_2NaYF_6:Eu ($\sim$1750 cm^{-1}). Several processes are available for the depopulation of the $(^5D_1)\Gamma_4$ state, besides the radiative mechanism. Multiphonon relaxation from $(^5D_1)\Gamma_4$ to $^5D_0\Gamma_1$ in Cs_2NaYF_6:Eu is possible via the emission of five phonons (such as $2\nu_5 + 3\nu_1$). Thermally activated non-resonant cross-relaxation processes such as

$$(^5D_1)\Gamma_4 + (^7F_0)\Gamma_1 + \text{phonon} \rightarrow (^5D_0)\Gamma_1 + (^7F_3)\Gamma_x$$

where x is 2, 4 and 5 may quench $^5D_1$. At higher temperatures a $^5D_1$-to-$^5D_0$ cross-relaxation process is possible in which the neighbour ion is initially in the $(^7F_1)\Gamma_4$ state and a τ_{2g} lattice phonon is emitted. The mechanism of the relaxation from $^5D_1$ to $^5D_0$ is independent of Eu^{3+} concentration at 4 K (table 7). It is interesting that at 4 K, the $^5D_1$ decay time was found to be shorter than the $^5D_0$ rise time. Although this suggests the cooperation of a long-lived intermediate state in populating $^5D_0$, we are unable to provide an explanation for this observation at this stage.

4. Conclusions

Cs_2NaYF_6 may be more readily synthesized by the hydrothermal method than by the solid-state reaction between CsF, YF_3 and NaCl, where it only exists over a narrow temperature range [47]. It can accommodate Eu^{3+} at low concentration at a perfectly octahedral site at 4 K, but the splitting of MD origins at low temperature in $Cs_2NaY_{0.8}Eu_{0.2}F_6$ shows that Eu^{3+} is situated in a lower-symmetry environment in the latter case. The vibrational behaviour and electronic spectra of Eu^{3+}-doped Cs_2NaYF_6 have been analysed and are

consistent with the spectra of $Cs_2NaEuCl_6$ [37] and Cs_2NaYCl_6:Eu [45]. The derived energy-level scheme is in agreement with the (less complete) results of Amberger and co-workers for Cs_2KYF_6:Eu [25] and Rb_2NaEuF_6 [26]. As deduced from the more complete data-sets of Berry *et al* [28] for Cs_2NaTbX_6, the CF parameters are clearly greater for X = F than X = Cl in Cs_2NaYX_6:Eu, but the uncertainties in the other parameter values derived from the relatively small data-sets of the present study prevent reliable comparisons. Due to the complexity of the optical spectra in the near-ultraviolet region, a more complete energy-level data-set might only be obtained via two-photon spectroscopy, and such experiments are planned. The temperature shifts of energy levels in Cs_2NaYF_6:Eu, and the shifts from Cs_2NaYF_6:Eu to Cs_2NaYCl_6:Eu, have been analysed in terms of changes in the CF and Slater parameters. The shifts differ from those in Cs_2UCl_6 because of the smaller CF and larger interelectronic repulsion in the lanthanide system. A preliminary study of the decay kinetics of the ^5D_J ($J = 0, 1, 2$) levels shows weak concentration quenching of the $^5D_2$ emission, thermally assisted quenching of the $^5D_1$ emission, and temperature- and concentration-independent behaviour of the $^5D_0$ emission. This is generally in accordance with the behaviour of Cs_2NaYCl_6:Eu, except that the cross-relaxation process which quenches the $^5D_2$ emission is more efficient.

Acknowledgments

PAT thanks Mr Pei Zhi-wu for technical support, and the HKUGC for funding under RG No 9040098.

References

[1] Tanner P A, Kumar V V R K, Jayasankar C K and Reid M F 1994 *J. Alloys Compounds* **215** 349
[2] Moran D M, May P S and Richardson F S 1994 *Chem. Phys.* **186** 77
[3] Bettinelli M and Flint C D 1990 *J. Phys.: Condens. Matter* **2** 8417
[4] Bettinelli M and Flint C D 1991 *J. Phys.: Condens. Matter* **3** 4433
Bettinelli M and Flint C D 1991 *J. Phys.: Condens. Matter* **3** 7053
[5] Tanner P A, Chua M and Reid M F 1995 *J. Alloys Compounds* **225** 20
[6] Morss L R, Siegal M, Strenger L and Edelstein N M 1970 *Inorg. Chem.* **39** 1771
[7] Aléonard S and Pouzet C 1968 *J. Appl. Crystallogr.* **1** 113
[8] Védrine A, Besse J-P, Baud G and Capestan M 1970 *Rev. Chim. Minerale* **7** 593
[9] Siddiqi I and Hoppe R 1970 *Z. Anorg. Allg. Chem.* **374** 225
[10] Feldner K and Hoppe R 1980 *Z. Anorg. Allg. Chem.* **471** 131
[11] Meyer G 1982 *Prog. Solid State Chem.* **14** 141
[12] Aull B F and Jenssen H P 1986 *Phys. Rev.* B **34** 6647
[13] Khaïroun S, Tressaud A, Grannec J, Dance J M and Yacoubi A 1988 *Phase Transitions* **13** 157
[14] Selgert P, Lingner C and Lüthi B 1984 *Z. Phys.* B **55** 219
[15] Veenendaal E J, Brom H B and Ihringer J 1982 *Physica* B **114** 31
[16] Ihringer J 1982 *Solid State Commun.* **41** 525
[17] Tressaud A, Khaïroun S, Chaminade J-P and Couzi M 1986 *Phys. Status Solidi* a **98** 417
[18] Couzi M, Khaïroun S and Tressaud A 1986 *Phys. Status Solidi* a **98** 423
[19] Urland W 1979 *Z. Naturf.* a **34** 1507
[20] Urland W 1980 *Z. Naturf.* a **35** 403
[21] Urland W, Feldner K and Hoppe R 1980 *Z. Anorg. Allg. Chem.* **465** 7
[22] Lifshitz A I, Voronov V N and Buznik V M 1981 *J. Struct. Chem.* **22** 127
[23] Veenendaal E J and Brom H B 1982 *Physica* B **113** 118
[24] Merchandt P, Grannec J, Chaminade J-P and Fouassier C 1980 *Mater. Res. Bull.* **15** 1113
[25] Amberger H-D 1980 *Z. Anorg. Allg. Chem.* **467** 231
[26] Thompson L C, Kuo S C and Amberger H-D 1991 *Eur. J. Solid State Inorg. Chem.* **28** 187
[27] Acevedo R, Tanner P A, Meruane T and Poblete V 1986 *Phys. Rev.* B **54** 3976

[28] Berry A J, McCaw C S, Morrison I D and Denning R G 1996 *J. Lumin.* **66+67** 272
[29] Satten R A, Schreiber C L and Wong E Y 1965 *J. Chem. Phys.* **42** 162
[30] Tanner P A and Krishnan J 1993 *Appl. Spectrosc.* **47** 1522
[31] Tanner P A, Chua M and Reid M F 1993 *Chem. Phys. Lett.* **209** 539
[32] Goryunov A V, Popov A I, Khaidukov N M and Fedorov P P 1992 *Mater. Res. Bull.* **27** 213
[33] Becker R, Lentz A and Sawodny W 1976 *Z. Anorg. Allg. Chem.* **420** 210
[34] Amberger H-D 1978 *Inorg. Nucl. Chem. Lett.* **14** 491
[35] Gutowski M, Boldyrev A I, Simons J, Rak J and Blazejowski J 1996 *J. Am. Chem. Soc.* **118** 1173
[36] Lentz A 1974 *J. Phys. Chem. Solids* **35** 827
[37] Tanner P A and Liu Y-L 1994 *J. Alloys Compounds* **204** 93
[38] Sinkovits R S and Bartram R H 1991 *J. Phys. Chem. Solids* **52** 1137
[39] Selgert P, Lingner C and Lüthi B 1984 *Z. Phys.* B **55** 219
[40] Tanner P A and Shen M-Y 1994 *Spectrochim. Acta* A **50** 997
[41] Chodos S and Satten R A 1975 *J. Chem. Phys.* **62** 2411
[42] O'Leary G P and Wheeler R G 1970 *Phys. Rev.* B **1** 4409
[43] Chodos S L, Black A M and Flint C D 1976 *J. Chem. Phys.* **65** 4816
[44] Stranger R, Moran G, Krausz E, Güdel H and Furer N 1990 *Mol. Phys.* **69** 11
[45] Morley J P, Faulkner T R and Richardson F S 1982 *J. Chem. Phys.* **77** 1710
[46] Reid M F and Richardson F S 1985 *J. Chem. Phys.* **83** 3831
[47] Mroczkowski S and Dorain P 1985 *J. Less-Common Met.* **110** 259